



Attribution of Deep Western Boundary Current variability at 26.5°N



Christopher S. Meinen^{a,*}, Silvia L. Garzoli^{a,b}

^a NOAA/Atlantic Oceanographic and Meteorological Laboratory, 4301 Rickenbacker Causeway, Miami, FL 33149, USA

^b Cooperative Institute for Marine and Atmospheric Studies, University of Miami, 4600 Rickenbacker Causeway, Miami, FL 33149, USA

ARTICLE INFO

Article history:

Received 7 March 2013

Received in revised form

10 April 2014

Accepted 29 April 2014

Available online 22 May 2014

Keywords:

Deep Western Boundary Current

MOC

PIES

Volume transport

North Atlantic Ocean

Variability

ABSTRACT

Observed variations in the Deep Western Boundary Current (DWBC) at 26.5°N, which carries the deep limb of the Atlantic Meridional Overturning Circulation (MOC), have been shown to greatly exceed in magnitude the variations of the overall basin-wide MOC, with strong variability at a range of time scales from weeks to multiple-months. Attribution of these strong DWBC variations will be crucial for understanding variations in the MOC itself. Nevertheless, despite many years of moored observations of the DWBC at 26.5°N, understanding of these variations has been elusive. Two years of observations from a high horizontal resolution array of pressure-equipped inverted echo sounders are used together with output from a modern high-resolution numerical model to investigate the mechanisms behind these $\pm 20 \times 10^6 \text{ m}^3 \text{ s}^{-1}$ volume transport variations. The model and observational results together suggest that the strongest variations cannot be explained solely via either of the two most commonly proposed mechanisms – meandering or pulsation of the DWBC. The dominant mechanism appears to be propagation of Rossby Wave-like structures into the region from the east, and it is the impact of these features in the region that yield the largest transport anomalies. These waves have been observed and discussed in the past – however their key role as the dominant source of DWBC variability has not previously been recognized. The implications of these results are also discussed in the context of future observing systems for the DWBC.

Published by Elsevier Ltd.

1. Introduction

Since it was first discovered in the 1950s, the Deep Western Boundary Current (DWBC) has intrigued the oceanographic community due to the many differences between the DWBC and the better-known surface currents (e.g., Stommel, 1957; Stommel and Arons, 1960; Swallow and Worthington, 1961). The discovery of the crucial role the DWBC plays in the Meridional Overturning Circulation (MOC), and the growing understanding of the importance of variability of the MOC (e.g., Vellinga and Wood, 2002; Stouffer et al., 2006) have encouraged further study of the DWBC (e.g., Johns et al., 2008; Toole et al., 2011). At several locations along its inter-hemispheric transit, key results on the pathway and time scales of variability of the DWBC have been discovered using Lagrangian floats (e.g., Bower et al., 2009, 2011), hydrographic sections (e.g., Molinari et al. 1998; van Sebille et al. 2011) and moored instruments (e.g., Lee et al., 1996; Dengler et al. 2004; Schott et al. 2005). Despite the significant resources that have

been applied to the study of the DWBC, however, there are many aspects of its nature that remain to be discovered.

One location where considerable effort has been expended to study the DWBC is at 26.5°N where the DWBC flows southward just east of the Bahamas Bank. Observations of the DWBC started in this area in the 1970s using Lagrangian floats (Riser et al., 1978), continued in the 1980s and 1990s with tall taut-line current meter moorings (e.g., Lee et al., 1990, 1996) and horizontal electric field recorders (Chave et al., 1997), and still continue to this day with dynamic height moorings (e.g., Johns et al., 2008) and pressure-equipped inverted echo sounders (Meinen et al., 2004, 2006, 2013). The studies in the late 1980s and early 1990s were perhaps the first fairly comprehensive measurement systems for looking at the time variability of the transport of the DWBC at this location. However while these studies produced quite a few interesting results on the mean transport, the spatial structure of the DWBC, and the annual cycle of the DWBC transport, these studies also resulted in some contradictory explanations for the observed DWBC variations. In particular, while it was observed that there were westward propagating Rossby Wave-like features entering the region, the greatest debate relating to the transport of the DWBC was over whether the large northward transport anomalies that were observed (i.e., periods where the southward transport of

* Corresponding author. Tel.: +1 305 361 4355; fax: +1 305 361 4412.

E-mail address: Christopher.Meinen@noaa.gov (C.S. Meinen).

the DWBC along the continental slope seemed to ‘disappear’ were associated with offshore meandering of the southward DWBC transport core (e.g., Lee et al., 1996) or whether these anomalies were associated not with horizontal movement of the DWBC core but were instead associated with pulsation (i.e., transport fluctuations) of the DWBC core itself (e.g., Chave et al., 1997).

Understanding of the mechanisms causing DWBC variability at 26.5°N has become more important because this latitude is the location of the first trans-basin mooring array for observing the total full-water-column meridional overturning circulation (MOC; e.g., Cunningham et al., 2007; Kanzow et al., 2007, 2010; Johns et al., 2011; Rayner et al., 2011). Attribution of the observed MOC changes will require insight into the mechanisms associated with changes in the constituent limbs of the cell, including the deep limb carried by the DWBC. There will be little purpose to monitoring the basin-wide MOC for changes if it proves impossible to understand the mechanisms associated with those changes when they are observed.

A recent study at this location (Meinen et al., 2013) has demonstrated that the southward deep transport associated with the DWBC (integrated from 800 to 4800 dbar) has baroclinic and barotropic¹ flows each having peak-to-peak variations exceeding 40 Sv ($1 \text{ Sv} = 10^6 \text{ m}^3 \text{ s}^{-1}$) on time scales ranging from a few days to a few months, and this flow variability remains strong regardless of whether the transport is integrated only a few hundred km from the continental slope or if it is integrated from the slope all the way out to the western flank of the Mid-Atlantic Ridge. To date it has proven difficult to definitively identify the mechanisms behind the strong variations observed at 26.5°N. In the present study, additional observations are used to improve the horizontal resolution of the observing array and thereby enhance understanding of those mechanisms. During September 2006–September 2008 two additional moorings were deployed in the region immediately offshore of the mean DWBC location, providing better horizontal resolution than at any previous time, in an endeavor to obtain additional information on the dynamics of the observed DWBC transport variability. This augmented data set, together with output from the Ocean general circulation model For the Earth Simulator (OFES) model, is used to further interpret the observed transport variability and to ascertain its causes.

2. Data and methods

2.1. Description of the observations

The observational component of this analysis is dependent on two primary types of measurements as well as some ancillary data sets. The primary measurements are of bottom pressure and round-trip acoustic travel time, both made by pressure-equipped inverted echo sounders (PIES). The first travel time and bottom pressure observations of the DWBC at this location were collected as part of a pilot experiment in 1996–1997; when they were compared to concurrent direct current meter data they were shown to be able to accurately capture the meridional velocity and transport in the deep (800–4800 dbar) levels (Meinen et al., 2004). A new experiment monitoring the DWBC using PIES at this location began in 2004 and continues to the present

(Meinen et al., 2006, 2013). During September 2006–September 2008 the long-term array was augmented with three additional instruments, one PIES and two IES (the “IES” also measures travel time but lacks the bottom pressure gauge), in the region just offshore of the mean DWBC location. One of the IES was not recovered – the final augmented array therefore included six PIES and one IES deployed in a line along 26.5°N east of Abaco Island in the Bahamas (see Fig. 1 and Table 1). The main array has the goal of collecting observations of both the shallow northward-flowing Antilles Current as well as the southward-flowing DWBC. This array operates in concert with related measurements of the Florida Current using a submarine cable (e.g., Meinen et al., 2010), thereby capturing both the upper and lower limbs of the MOC near the western boundary. The array also contributes to the basin-wide MOC array at 26.5°N (e.g., Cunningham et al., 2007; Kanzow et al., 2007; Meinen et al., 2013). The 2006–2008 augmentation of the PIES array was designed specifically to focus on understanding the variability of the DWBC observed during the first few years of the main PIES array; this study will focus on the two year period of high-density PIES (and IES) observations in the DWBC between sites B, C, D, and E as well as the augmentation sites D3 and D4 (Fig. 2).

2.2. From travel time to volume transports

There is a significant body of literature describing the analysis of PIES data (e.g., Rossby 1969; Watts and Rossby 1977; Garzoli and Gordon, 1996; Meinen and Watts, 2000; Watts et al., 2001; Donohue et al., 2010), so the techniques will be only briefly reviewed here with the appropriate citations to other articles provided for the details. The acoustic measurement of a PIES is based on the round-trip travel time of a 12 kHz (or 10 kHz, in older models) sound pulse from the bottom moored instrument up to the sea surface and back (e.g., Rossby, 1969; Watts and Rossby, 1977). By itself the travel time measurement is of little use, however when combined with hydrographic observations from the region the travel time measurement becomes quite powerful. The travel time measurements presented here were combined with hydrography-derived 2-dimensional look-up tables of temperature, salinity, and density as functions of pressure and simulated travel time. These look-up tables were created using 458 conductivity-temperature-depth (CTD) profiles collected between 1984 and 2008 in the region; the tables were calculated following the ‘Gravest Empirical Mode’, or GEM, technique first developed by Meinen and Watts (2000). Combining the PIES travel time records with the hydrography-derived GEM look-up tables yields daily time series of full-water-column profiles of temperature, salinity, and density²; the latter can be vertically integrated to produce dynamic height anomaly (geopotential height anomaly) profiles.

Differencing the dynamic height anomaly profiles between pairs of PIES yields full-water-column profiles of the component of the geostrophic velocity (relative to an assumed level of no motion) that is perpendicular to the line between the PIES. Previous studies in this region, however, have demonstrated that the absolute transport of the DWBC has no significant relationship to the geostrophic transport relative to any level of no motion one might select – therefore absolute transports are essential (e.g., Meinen et al., 2006, 2013). The bottom pressure measurements

¹ The terms “barotropic” and “baroclinic” have multiple accepted definitions in the literature (e.g., barotropic as ‘full depth vertical mean velocity’ or barotropic as ‘bottom velocity’). For this study the term “barotropic” is used to describe the full depth vertical mean, and “baroclinic” is the deviation from that mean. Note that while in this definition the baroclinic term integrated over the full water column has by construction a zero net transport, integrating the baroclinic flow over only a portion of the vertical water column yields a non-zero transport.

² Note: The look-up tables used here are slightly different than those used in the Meinen et al. (2013) study. In order to evaluate the data from Site A, which is roughly 1000 m deep, the GEM tables were calculated using travel time simulated between the surface and 1000 dbar, rather than surface to 3000 dbar as was used in the Meinen et al. (2013) study. This has a small but non-zero effect on the estimated temperature, salinity and density profiles determined from the PIES – these differences are not important for the purposes of the present study.

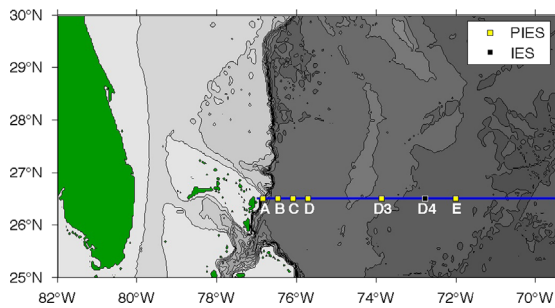


Fig. 1. Map of the study region illustrating the locations of the moored instruments used in this study. Mooring types are indicated in the legend, and blue line indicates the repeated hydrographic section that has been observed quasi-annually since 1984. White letters indicate site names. Bottom topography is shown from Smith and Sandwell (1997) with 500 m contour levels – Sites B, C, D and D3 are between 4500 m and 5000 m depths, while Sites D4 and E are between 5000 m and 5500 m.

Table 1

Longitudes (along 26°–30°N) where the PIES (and IES) moorings are located. Note the latitude for Site A is actually 26° 31' N. Also shown is the distance of each mooring from the continental slope, defined using the longitude of Site A.

Site name	Type of mooring	Longitude	Approximate depth (m)	Approximate distance from shelf (km)
A	PIES	76° 50'W	1065	0
B	PIES	76° 28'W	4804	37
C	PIES	76° 05'W	4761	74
D	PIES	75° 42'W	4690	113
D3	PIES	73° 52'W	4717	296
D4	IES	72° 46'W	5118	405
E	PIES	72° 00'W	5233	481

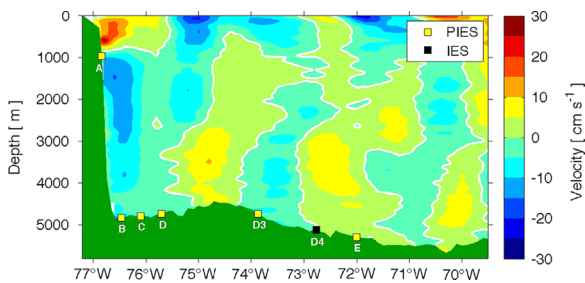


Fig. 2. Vertical section illustrating the locations of the moored instruments east of the Bahamas on the bottom topography. Green indicates the bottom topography, while white letters indicate the site names for the PIES and IES moorings. High spatial resolution DWBC data were collected at Sites B, C, D, D3, D4 and E for the period of time September 2006–September 2008. Filled contours are a schematic based on heavy smoothing of all meridional velocity sections collected along this line up through 2006 (both Pegasus and lowered-Acoustic Doppler Current Profiler – see Meinen et al., 2013 for more information); the velocity section is shown for illustration purposes only and should not be taken to perfectly represent the true mean due to inconsistent sampling in time/space and heavy smoothing involved in creating the schematic.

made by the PIES are the solution to this problem. Differencing the bottom pressure records from neighboring PIES provides an absolute near-bottom reference velocity, missing only the time-mean bottom velocity due to the well known ‘leveling’ problem (e.g., Watts and Kontoyiannis, 1990; Donohue et al., 2010). The bottom pressure gauges were differenced along this line and were added to time mean flows created based on historical current meter data in the region.³ The resulting time-varying absolute

geostrophic bottom velocities were then used to reference the relative velocity profiles determined from the travel time measurements and GEM fields (see Meinen et al., 2013, and references cited therein, for more details on obtaining absolute velocities from PIES). The result is daily, full-water-column, profiles of absolute velocity between each pair of PIES in the array. Because the Site D4 mooring was an IES only, meaning it lacked bottom pressure observations, it is used only for relative velocity discussions herein.

Based on historical hydrographic (e.g., Molinari et al., 1998; van Sebille et al., 2011) and mooring observations in the region (e.g., Meinen et al., 2013 and references therein), the DWBC volume transport is defined here as the integrated transport between sites B and E from 800 dbar and 4800 dbar (or the bottom where it is shallower than 4800 dbar). This broad horizontal range, much larger than the earlier integrations between sites B and D used, for example, by Lee et al. (1996), is selected specifically to capture as much of the southward flow as possible near the continental slope. Note that there is a small portion of the DWBC west of site B that is not captured in this integral – this is consistent with the earlier work of Lee et al. (1996) and others who also had no moored instruments in the narrow region west of Site B. The results herein are not sensitive to small (~ 100 – 300 dbar) changes in the bounding depth levels used for the integration, and evaluation of the deep flow west of site B indicates that the flows in that narrow region do not significantly change the character of the time series shown herein. Daily time series of transport are low-pass filtered using a second-order Butterworth filter with a 72-hour cut-off period, passed both forward and back to avoid phase shifting. A few time gaps (of less than 3 months) in selected travel time records were filled via a comparison with satellite altimetry observations as discussed in Appendix A. Shorter time gaps (of less than two weeks) were filled via linear interpolation.

2.3. Description of the model

Output from the Atlantic sector of the global Ocean general circulation model For the Earth Simulator (OFES) was kindly provided by the OFES group for use in this study. The OFES simulation was conducted on the Earth Simulator under the support of the Japan Agency for Marine-Earth Science and Technology (JAMSTEC). The OFES model is a massively-parallelized Mercator B-grid z -level system which is based on the NOAA/GFDL Modular Ocean Model version 3 – MOM3. The model has a horizontal resolution of 0.1° and it has 54 vertical levels. The model run that produced the output used here was spun up for 50 years with a monthly climatology calculated from NCEP/NCAR reanalysis fluxes (e.g., Masumoto et al., 2004) after which it was forced with daily mean NCEP/NCAR reanalysis data from the period 1950 through 2006 (Sasaki et al., 2008). For this study JAMSTEC provided a subset from 24 to 28° N, west of 10° W with every other horizontal grid point (i.e., every 0.2°); the time resolution provided was every 3 days over the final 27 years of the run. The output of the model was validated against the available concurrent hydrographic section and mooring data to the extent possible.

(footnote continued)

Because this paper focuses on a shorter time window, there are insufficient sections to do the same here. The transport means are slightly different as a result, however because the focus of this study is on the sources of variability, not the physics setting the mean, this is not a significant concern.

³ Note: The time mean flows used here are slightly different than those used in the Meinen et al. (2013) study. The Meinen et al. (2013) study supplemented the current meter time mean with information from lowered and shipboard Acoustic Doppler Current Profiler (ADCP) sections concurrent with the PIES observations.

Table 2

Results from the Empirical Orthogonal Function analysis of two-years of travel time data collected at sites B, C, D, D3, D4 and E. The upper table shows the percentage of variance explained by each one of the three dominant modes, the error associated with the mode, and the coherence between the variable and the mode (γ). In the lower table A indicates the amplitude of the mode.

Mode	%Var	Error(+,-)	γ (B)	γ (C)	γ (D)	γ (D3)	γ (D4)	γ (E)
1	48.12	0.28	0.85	0.86	0.85	0.14	0.05	0
2	27.12	0.16	0.04	0.05	0	0.4	0.61	0.44
3	14.28	0.08	0	0.02	0.01	0.4	0	0.38
Mode	%Var	Error(+,-)	A (B)	A (C)	A (D)	A (D3)	A (D4)	A (E)
1	48.12	0.28	-0.86	-1.07	-1.25	-0.09	-0.01	0
2	27.12	0.16	-0.01	-0.02	0	0.57	0.55	0.44
3	14.28	0.08	0	0.01	0	-0.78	0	0.48

3. Results

3.1. Zonal variability coherence and time scales

The additional deployments at sites D3 and D4 (see Fig. 2) significantly narrowed the span between the offshore instruments, thereby improving the zonal resolution of the array and allowing for the determination of the coherence between the array sites. To analyze first the observed in-phase spatial structure, an empirical orthogonal function (EOF) decomposition (e.g., Emery and Thomson, 1997) was conducted on the travel-time records at sites B, C, D, D3, D4 and E for the period of time from September 2006 to September 2008. Travel time is tightly (and nearly linearly) related to dynamic height anomalies, which are themselves representative of the baroclinic component of the motions. The amplitude and sampling error of the EOF modes were determined following Garzoli (1984) and North et al. (1982), respectively. The first three empirical modes explain 90% of the total variance of the system. Table 2 shows the percentage of variance accounted for by each of the first three EOF modes, the fraction of the variance of the j th variable explained by the i th empirical orthogonal function (Wallace and Dickinson, 1972), and the spatial amplitude of each mode at each mooring site. When these percentages of variance, with error estimates, do not overlap, the modes can be separated and physically interpreted as modes of variability. These calculations (see Table 2) indicate that the first three modes are significant.

The resulting time dependence and spectral character of the dominant modes are shown in Fig. 3. The EOF analysis indicates that 90% of the total variance of the system can be explained by three dominant modes. A strong semiannual period is observed both in the first mode (48% of the total variance) and in the second mode (27% of the total variance). The third mode (14% of total variance) indicates higher frequency oscillations in the bands 50–60 and 120–140 days, with strongest amplitudes observed at sites D3, D4 and E. The first mode is highly correlated to the observed variability at sites B, C and D, with maximum amplitude at D. The second mode is correlated to the variability at sites D3, D4 and E (Table 2). The travel time records are tightly related to profiles of dynamic height anomaly, and hence to the baroclinic structure/signals (while the barotropic components of the flow cannot be considered without incorporating the bottom pressure records). A similar EOF decomposition (not shown) was performed on the available pressure records at sites B, C, D, D3 and E, and it shows a similar pattern of correspondence of mode 1 to sites B, C and D, and mode 2 to the variations at sites D3 and E. The main result of this modal decomposition is that the in phase variability of both the travel time and bottom pressure signals are decoupled west and east of a location between sites D and D3 somewhere near 74–75°W. Because this longitude is roughly the location of

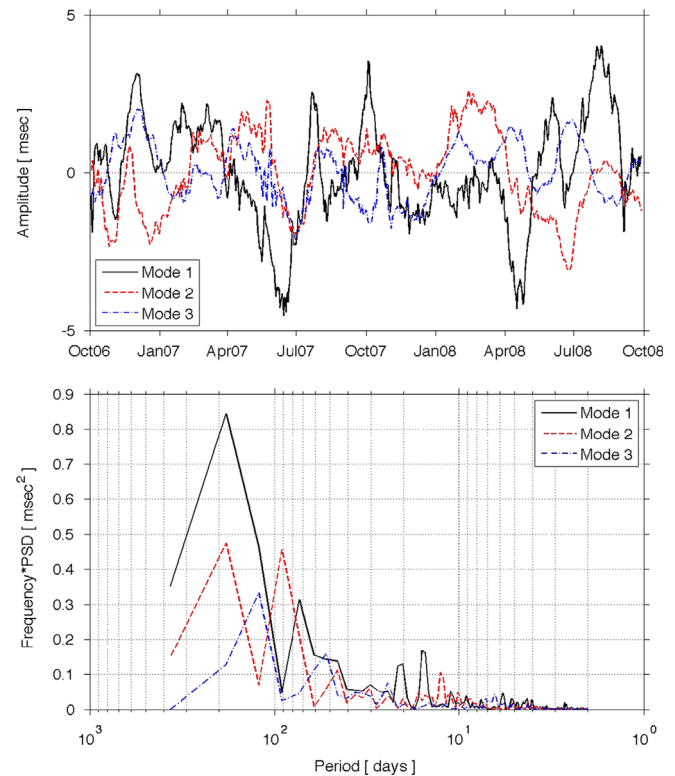


Fig. 3. Amplitude time series (top panel) and variance-preserving spectra (bottom panel) of the three dominant EOF modes determined from the travel time records at Sites B, C, D, D3, D4, and E.

the mean offshore edge of the DWBC (see the schematic in Fig. 2), this suggests that the flow variations within the DWBC mean domain are out of phase and decoupled from the motions to the east of that longitude.

Spectral analysis of the acoustic travel-time records (not shown) indicates the presence of energetic oscillations at all sites for periods in the bands 15–18 and 25–30 days. A strong peak in energy is also observed centered in the 70–90 day period band at all sites. Spectral analysis of the pressure records finds that they are dominated by a strong energetic peak at ~14 days and significant energy at different peaks in the period band from 20 to 90 days. Coherence between the pressure and travel time records ($0.5 \leq r \leq 0.7$) is modest, but significant, in the 10–20 day band and for periods of 50–60 days. The pressure and travel time records are uncorrelated at periods between 20 and 50 days and at periods larger than 60 days. It must be kept in mind that the velocity signals (both baroclinic and barotropic) are based on gradients between travel time or pressure signals at neighboring sites, not on the travel time or pressure signals at a given site. Note also that cross-spectral analysis between the sites shows highly coherent features at periods of 70–90 days – the sign of the very stable phases in this period band indicates westward propagation. Because there is evidence of strong propagating variability in this region, it is important to also evaluate the observed signals in a manner that allows for estimating phase propagation, as will be discussed shortly.

3.2. The volume transport

The full 5-year record of DWBC volume transport integrated from the shelf out to Site E is shown in Fig. 4. The DWBC transport exhibits significant variability, with a total peak-to-peak range of roughly 140 Sv and a standard deviation of 26 Sv. The record has no obvious annual cycle. A more detailed description of the full

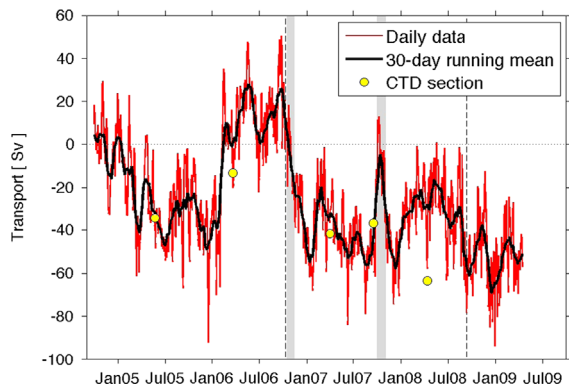


Fig. 4. Time series of DWBC absolute transport integrated between 800 and 4800 dbar and from Site B out to Site E. Red thin line indicates daily transport estimates, while black thick line indicates transports after the application of a 30-day running mean. Two gaps resulting from instrument failures have been filled using altimetry data as described in the Appendix A. Yellow circles indicate hydrographic (CTD) section geostrophic transport estimates where the barotropic flow component has been provided by the pressure differences from the PIES – hence they only represent a test/comparison of the baroclinic component of the flow. Vertical black dashed lines indicate the start and end of the higher resolution array deployment; gray shading indicates two events during the high resolution array period that are highlighted in the text.

5-year record as well as a discussion of the spectral character and statistical stability of the variability was presented in Meinen et al. (2013). Of particular interest for the present study are the periods of time where the DWBC reverses toward the north or has close to zero transport. The 5-year record (Fig. 4) shows several periods of near-zero or positive (northward) transports, with particularly long time periods in late-2004 to early 2005 and during April–October 2006. Recent studies in the region using tall mooring data (e.g., McCarthy et al., 2012) have found that some of these low DWBC transport events are barotropic in nature (i.e., they impact the deep and shallow layers), while others are associated only with shear changes between the deep layers. The recent Meinen et al. (2013) study demonstrated that the PIES could capture the net transport changes well in these types of events, but some of the vertical structure details within the deep layer were not as well represented in the PIES data. The focus in this study is on the net deep flows, which the PIES capture well. During the period of time covered by the high-resolution observations (September 2006–September 2008), there are several large net northward anomaly episodes (Fig. 4): focus herein will be on two of the largest events in late 2006 and in boreal autumn 2007 (highlighted with gray shading in Fig. 4). In what follows, the analysis will center on understanding the dynamics that cause these large anomalies/changes in transport.

The time series of absolute transport integrated between each pair of moorings and from 800 to 4800 dbar is shown as a Hovmöller diagram in Fig. 5 (left panel) as a function of time and space for the two years of high resolution data.⁴ Note that, as the horizontal spacing between PIES sites is irregular, the amplitude of signals moving between pairs of PIES is not the same. To look for propagating features in the left panel of Fig. 5, one must focus on moving signals of the same sense (i.e., northward anomalies or southward anomalies). To aid in visualization, a second contour plot is shown (Fig. 5, right panel) that shows a Hovmöller blow-up of the travel time anomalies centered on the first event highlighted in the left panel using all of the instruments (including Site D4). The transport results (Fig. 4) indicate

anomalous northward flow in the DWBC layer at the western boundary for the periods of time September–November 2006 and for October–December 2007. While there is a range of different types of events that occur within the study region, the transport Hovmöller diagram and the travel time contour plot (Fig. 5, left and right panels) clearly suggest that the large observed northward flow anomalies identified above are related to the westward propagation of wave-like features from the interior of the basin (illustrated via the black arrows in Fig. 5; note that the black arrow in the right panel has the identical slope as the first arrow in the left panel). The cross-spectral analysis of the dynamic height series at all sites (not shown) confirms that a westward propagation is observed in the period band 70–90 days with a speed of propagation of 5–7 cm/s (a result that is supported by the model output that will be presented shortly). While the observational data set is noisy, there is no clear indication during the two-year record of the strong southward DWBC flow ever moving smoothly eastward. This is a crucial result, as it appears to exclude one of the key mechanisms, meandering, previously hypothesized to explain the DWBC transport variability observed at this location.

Lee et al. (1996), using several years of mooring data at up to five sites along this line, suggested that the periods when the southward transport integrated out to Site D disappeared were the result of westward propagating Rossby Wave-like features entering the region and the DWBC meandering further offshore. With only one traditional current meter mooring⁵ offshore of Site D, Lee et al. (1996) could not conclusively document this offshore DWBC. With the additional sites shown herein, coupled with the geostrophy-based fully-integrating transport methods, it can be stated that there is no evidence of such offshore movement during the events observed here. Such meanders would require the DWBC transport core to shift eastward, and hence eastward propagation would appear in a Hovmöller diagram such as that shown in Fig. 5. Chave et al. (1997) deployed horizontal electric field recorders (HEFR) east of the Lee et al. (1996) current meter moorings, and they reported seeing no indication of the DWBC transport core offshore of the current meter moorings during the periods when Lee et al. (1996) had suggested that the DWBC had meandered offshore (note the HEFR measure full-water-column mean velocity, not just the deep layer). It should also be kept in mind that the HEFR measurements, while representing velocity profiles that are ‘averaged’ over a horizontal range that is on the order of the water depth, still represent the equivalent of horizontal point measurements in the context of a sparse horizontal array when the moored instruments are many tens of kilometers from one another. As such the HEFR array could easily have missed significant flow between the sites. The fact that the geostrophic (integrating) methods used here find a result consistent with that of Chave et al. (1997) is strong evidence that Chave et al. (1997) were correct in disputing the meandering hypothesis. The lack of any evidence for eastward propagation during the large transport anomalies (Fig. 4) suggests that the DWBC does not meander offshore at this location during this two-year period, even though the large reductions in southward transport are clearly observed.

Even with the higher resolution available with the addition of Sites D3 and D4, the observational array still is somewhat limited as it only produces four integrated velocity time series between pairs of neighboring PIES. To further investigate westward

⁴ Recall that because site D4 was only an IES, i.e., that it had no bottom pressure data, it cannot be used for absolute transport calculations.

⁵ The earlier studies used current meter moorings to observe the flows. Current meters themselves are point measurements in terms of horizontal resolution, so horizontally confined signals which are between neighboring current meter moorings are invisible to those moorings. The geostrophy-based methods used herein are inherently horizontally integrating, so transport signals cannot be ‘missed’ between mooring sites as they could with horizontally-sparse current meter mooring arrays.

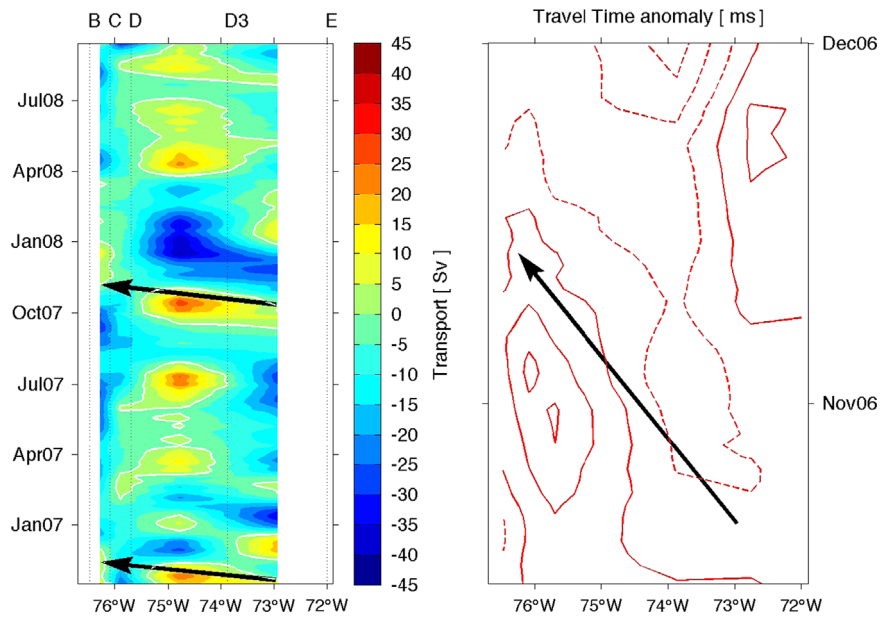


Fig. 5. Left: The time series of absolute transport integrated between each pair of moorings (and between 800 and 4800 dbar) is shown in panel as a function of time and space for the two years of high resolution data. White contour indicates zero flow. Transports have been smoothed with a 31-day running mean to highlight longer period signals. Black arrows are shown solely to highlight westward propagation of northward anomalies. Locations of the PIES are noted by vertical dotted lines. Note: The distance between PIES sites varies, and as a result larger transport signals tend to be observed in the larger spans such as between Sites D and D3. Right: Contour plot of the travel time anomalies (relative to the record length mean) measured by the PIES; the time period shown highlights the time period of the first large event shown in the left panel. Dashed contours indicate negative anomalies, while solid contours indicate positive anomalies; contour interval is 2 ms.

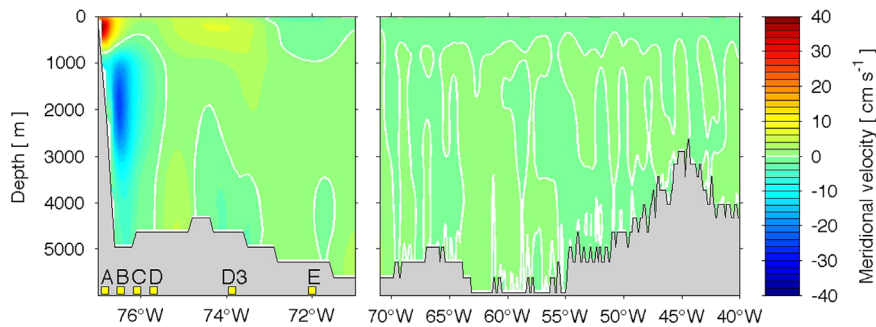


Fig. 6. Mean meridional velocity (1980–2006) along 26.5°N from the OFES model run described in the text. White contour denotes zero velocity; gray shading denotes the ocean bottom. Nominal locations of the PIES (yellow squares) are noted in the left panel. Note the difference in horizontal scale between the left ‘detail’ panel and the right ‘basin interior’ panel.

propagation of the observed transport signals, and the possible relationship to the displacements of the core, the product from a 0.1° resolution run from the Ocean general circulation model For the Earth Simulator (OFES) was analyzed. The mean velocity field in the model (1980–2006) is shown in Fig. 6 for the western side of the Atlantic basin out to the Mid-Atlantic Ridge. In the model, strong velocities are found only west of 70°W. The DWBC is observed west of Site D in the model field centered between Sites B and C, and between roughly 800 and 4800 dbar, which is consistent with present-day and historical observations. Subsampling the model to the horizontal resolution of the real world PIES array results in noisier sections (not shown) that show similar character and propagation patterns to the observed PIES data, however the strength of the model is that it has much better horizontal resolution (and a longer record), so the focus here is on analyzing the full available resolution of the model output.

Hovmöller diagrams of the model volume transport integrated vertically over the same depth range as the observations (from 800 to 4800 m) at 26.5°N are shown in Fig. 7; the 27 years of OFES output (1980–2006) are separated into three 9-year segments. There are several periods of time in which northward transport is

observed west of Site D (i.e., in the longitude band where the southward core of the DWBC is generally observed). Focusing on the larger features west of Site D with the high horizontal resolution available from the model, it is clear that all events are resulting from westward propagation from the interior of the basin. There is no evidence for eastward propagation that would be required for meandering – which would appear as southward flow smoothly shifting eastward with time in the Hovmöller plots. There are cases where there is strong southward flow east of Site D (e.g., early 1986, early 2003), however in all cases these are associated with strong features (of roughly equivalent transport to the mean DWBC) that have propagated westward into the region from the interior. The mean westward signal propagation is 4–5 cm/sec in the model, which is slightly slower than but comparable to what is observed in the two years of observations from the augmented array.

Focusing on the velocity and transport structure during the January 2002 event in the model provides further understanding. Comparing the January 2002 average meridional velocity section (Fig. 8) to the 27-year average section (Fig. 6), the “DWBC main core” appears to be located east of its average location. Inshore of

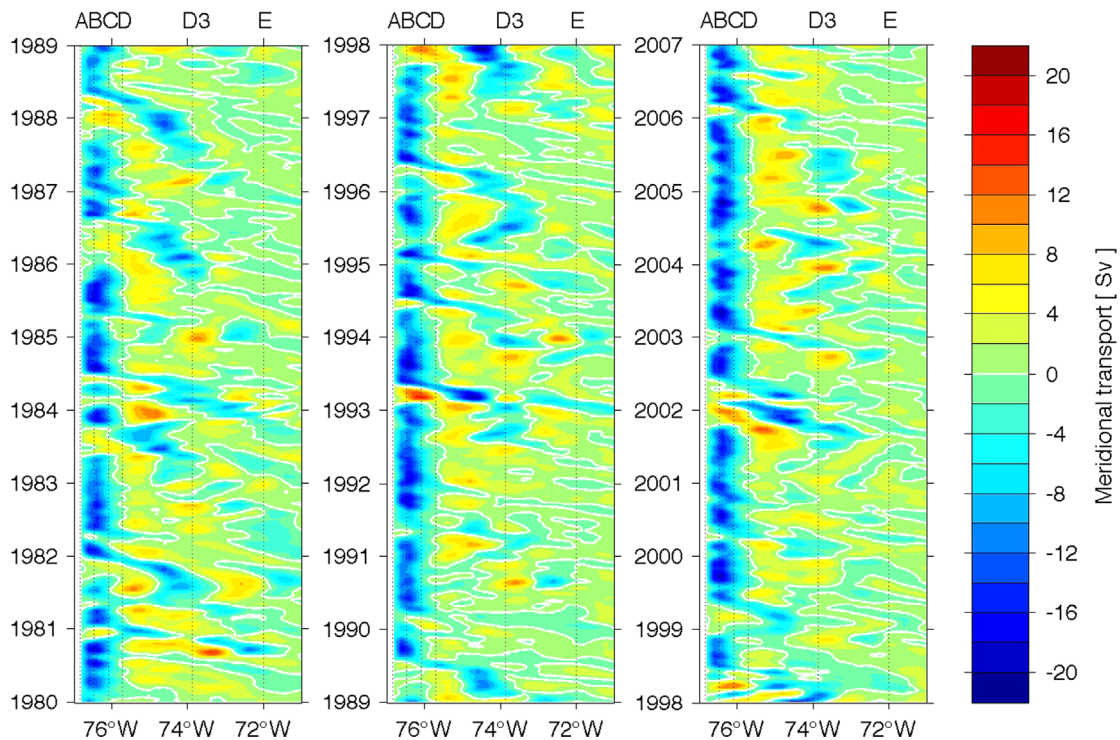


Fig. 7. Hovmöller diagrams are shown illustrating the OFES meridional volume transport integrated from 800 to 4800 m and between model grid points along 26.5°N. White contours indicate zero flow. Transports are separated into 9-year segments over the 27 years of available OFES output (1980–2006). Nominal locations of the PIES are denoted by vertical black dotted lines – site names are indicated along the top of each panel.

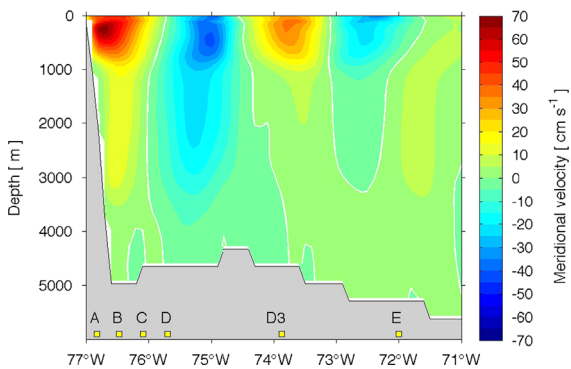


Fig. 8. Mean meridional velocity (averaged over January 2002 only) along 26.5°N from the OFES model run described in the text. White contour denotes zero velocity; gray shading denotes the ocean bottom. Nominal locations of the PIES (yellow squares) are noted.

this southward core, northward flow is observed over the full water column. East of the core an anticyclonic circulation is also observed. To better determine the cause of this apparent displacement, maps of the meridional volume transport as a function of longitude and latitude were created both for the 800–4800 dbar layer (DWBC) and the 0–800 dbar layer (Fig. 9). The maps illustrate several alternating bands of meridional flow, reflecting cyclonic and anticyclonic circulation features at 24.5°N, 26.5°N, and 28°N roughly between 74°W and 76°W. The maps (Fig. 9, lower panels) suggest that the core of the DWBC is near the boundary at 28°N and that it is further east at 26.5°N. The Hovmöller diagram (Fig. 7) demonstrates that this was not a meander offshore, but an anticyclonic wave-like event of roughly equivalent transport magnitude to the mean DWBC propagating westward into the region.

Another key observation is that the same reversals in flow are observed in the upper layer, above 800 dbar (Fig. 9, top panels), indicating that the displacement is somewhat barotropic in nature.

This barotropic-style structure associated with the northward anomalies is also observed in the PIES data (not shown). The barotropic-type flow contradicts the expectations of the other leading hypothesized mechanism to explain the observed strong DWBC transport fluctuations. *Chave et al. (1997)*, in arguing that the transport decreases were not associated with meandering of the DWBC, hypothesized that the fluctuations were instead associated with ‘pulsation’ of the DWBC, i.e. intensifications and de-intensifications of the current in the deep layer. The barotropic nature of the observations detailed herein, however, argue against that explanation. No obvious reason explains why ‘pulsing’ variations in a buoyancy-forced DWBC would force concurrent changes in the transport of the upper layer (which is made up of different water masses circulating in what is essentially a different ‘gyre’). It should be noted that these features are not barotropic in the sense that there is no variation in depth at all. Figs. 8 and 9 suggest that the flow is aligned in the upper and deep layers, but the magnitude of the flow in the upper layer is higher than at depth, consistent with a combined barotropic and first baroclinic normal mode structure, which is sometimes referred to as an ‘equivalent barotropic’ structure.

The results of both the two-years of observations from the augmented PIES array and the longer (and more highly resolved) model record suggest, therefore, that the strong variations of the DWBC transport observed at 26.5°N near the Bahamas Bank are not due solely to meandering or to pulsation. The largest variations appear instead to be related to the propagation of strong wave-like signals westward into the observation region. The observed propagation speeds of 5–7 cm s⁻¹ are a bit faster than the simple theoretical first-mode baroclinic Rossby Wave speeds predicted for this latitude, but they are consistent with the propagation speeds of real-world first-mode baroclinic Rossby Waves that have previously been observed in satellite altimeter data (e.g., *Chelton and Schlax, 1996; Osychny and Cornillon, 2004*) and in the earlier mooring results by *Lee et al. (1996)*. The transport results presented in *Meinen et al. (2013)* are also

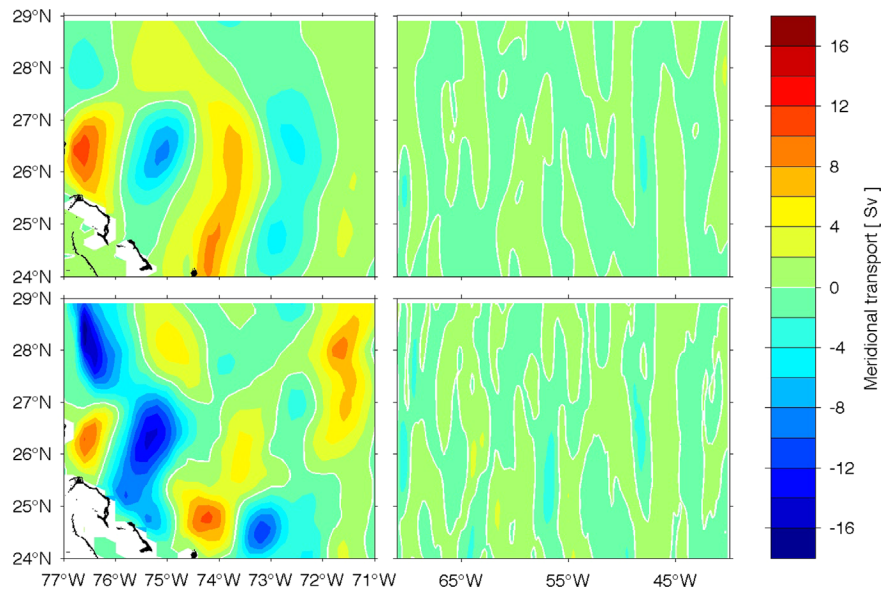


Fig. 9. Maps of the January 2002 time-mean OFES meridional volume transport for the upper layer (integrated from the surface to 800 m; top panels) and for the DWBC layer (integrated from 800 to 4800 m; bottom panels). The left panels provide high zonal resolution near the boundary. The right panels illustrate the basin interior from 70°W out to the Mid-Atlantic ridge – note the different zonal scales between left and right panels. Land is shown in black – regions with no contours indicate areas where the model topography is less than 800 m deep (top) or 4800 m deep (bottom). White contours indicate zero meridional transport.

instructive in this regard. In that study the transport in the 800–4800 dbar layer was integrated from the continental shelf out to the western side of the Mid-Atlantic Ridge (MAR). The strong anomalously northward flows noted in this study still appear in the transport integrated from the continental slope out to the west side of the MAR shown in the Meinen et al. (2013) study, albeit somewhat more weakly (anomalies of ± 20 Sv in the deep western basin, whereas the basin-wide upper limb MOC variations are only ± 10 Sv). This suggests that while the Chave et al. (1997) idea of pulsation near the boundary is not supported, the deep flow in the western half of the basin may be ‘pulsing’ in a sense. The Meinen et al. (2013) study noted that the variations in the western half of the Atlantic basin significantly exceed those of the basin-wide Meridional Overturning Circulation, which suggests that the deep layer flow east of the MAR must be counteracting some of the observed deep variability west of the MAR. The results of the present study draw a strong connection between the observed Rossby Wave-like westward propagating features and these strong half-basin transport fluctuations.

4. Conclusions

Two years of data from a line of PIES confirm previous results indicating that the barotropic and baroclinic components of the DWBC are uncorrelated, reinforcing the importance of observing both components of the flow in order to accurately measure the transport of the current. Furthermore these results from the high spatial resolution array indicate that deep flows east and west of 74–75°W are decoupled, oscillating out of phase as different modes. The data have also been used in concert with output from a high resolution global model to argue that the dominant signal resulting in the largest transport signals in the DWBC at 26.5°N is the propagation of Rossby Wave-like features westward into the boundary region. Taken together, the data and model results do not appear to be consistent solely with either of the earlier hypothesized ideas that offshore meandering or along-boundary pulsation would explain the strong 20+ Sv anomalous northward weeks-to-months transport signals observed routinely in the region. These strong anomalous northward flows instead appear

to be the superposition of the strong anticyclonic wave-like signatures over the southward flowing DWBC.

The character of the westward propagating features are consistent with previous satellite and in situ observations of first baroclinic mode Rossby Waves, although like the earlier satellite observations the propagation speeds are slightly faster than theory predicts ($5\text{--}7\text{ cm s}^{-1}$). The dominant period of these events is in the 70–90 day window, although transport variations are observed at both longer and shorter periods. The strong northward anomalies are somewhat barotropic in nature in that they are observed clearly both below 800 dbar (in the DWBC layer) and above 800 dbar (which is more characterized by the wind-driven subtropical gyre).

There are significant implications from these results, in that they demonstrate the challenges of using a limited-length mooring array to observe the transport of a specific current in an eddy/wave rich environment. Without observations outside of the location of the current (in this case offshore of the boundary region), it is possible to erroneously interpret changes in the flow as changes in the current itself, while they may instead be associated solely with propagation into the observation array of strong signals from elsewhere (in this case propagating features with transports as large as that of the current being studied). Based on the wealth of observations demonstrating the eddy rich nature of the global ocean, this becomes a serious interpretation issue for all ocean current transport observations from both snapshot sections and moored arrays.

Acknowledgments

The authors would like to express their appreciation to the ship officers and crew of the R/V Seward Johnson, R/V Cape Hatteras, and the NOAA Ship Ronald H. Brown for their assistance in maintaining the NOAA Western Boundary Time Series – Deep Western Boundary Current array during this time period. Support for this study was provided by the NOAA Climate Program Office and the Atlantic Oceanographic and Meteorological Laboratory, with some additional piggy-back ship time provided on cruises funded by the NSF Physical Oceanography Program (Grants

OCE0241438 and OCE0728108). Qi Yao and Rigoberto Garcia provided outstanding assistance in processing and analyzing the data used herein, Francis Bringas aided in obtaining the altimetry data, and the NOAA-AOML Physical Oceanography Division instrumentation group provided operational assistance deploying and recovering the instruments. The OFES model output was kindly provided by Hide Sasaki at JAMSTEC. Greg Foltz, George Halliwell and two anonymous reviewers provided several helpful comments for improving earlier versions of this manuscript.

Appendix A. Filling time gaps in the in situ records using altimetry

The travel time record at Site E had several gaps due to equipment malfunction. Site E was deployed close to an Envisat altimeter track, leading to the possibility of filling the gaps using altimetry data. The sea surface height anomaly (SSHA) measured via altimetry includes both baroclinic and barotropic signals (e.g., Hendry et al., 2002), and previous analyses in this region have demonstrated that the barotropic and baroclinic components of

the flow are uncorrelated (e.g., Kanzow et al., 2007), so altimetry alone cannot be used to simulate both the baroclinic and barotropic contributions to SSHA. As the baroclinic signal (relative to the bottom) is generally the larger contribution to SSHA, the altimeter data was used to fill gaps in the baroclinic time series – i.e., the travel time record. Because the travel time record from the PIES is related only to the baroclinic structure relative to the bottom, using altimetry-measured SSHA to fill gaps in the travel time record will result in aliasing of the barotropic signal into the travel time record. As such, this method can never be ‘perfect’, however the SSHA signal can be compared to the travel time signal during periods when both are available in order to quantify the imperfections. After filtering and sub-sampling the daily travel time record to fit the time resolution of the temporally and spatially gridded SSHA data, the resulting time series were compared. The correlation between SSHA and travel time at Site E during periods when both are available is significant, with a correlation coefficient $r=0.8$ (Fig. A1, top panel). This suggests that a linear relationship between the two will capture roughly 64% of the total variance, with the remaining 36% relating to barotropic signals, noise in the actual measurements, and errors resulting from the interpolation of the altimeter data from the ground track to the actual PIES site. Nevertheless, given the gaps in the Site E record are not particularly long, using the SSHA data in this manner seems reasonable. Using the linear relation between the two variables, travel time was derived from SSHA (Fig. A1, middle panel), and was fit into the time gaps in the Site E travel time record (Fig. A1, bottom panel). As noted above, because the same SSHA signal cannot be used to fill gaps in both the travel time and bottom pressure record, the missing bottom pressure data during these gaps was simply filled using linear interpolation.

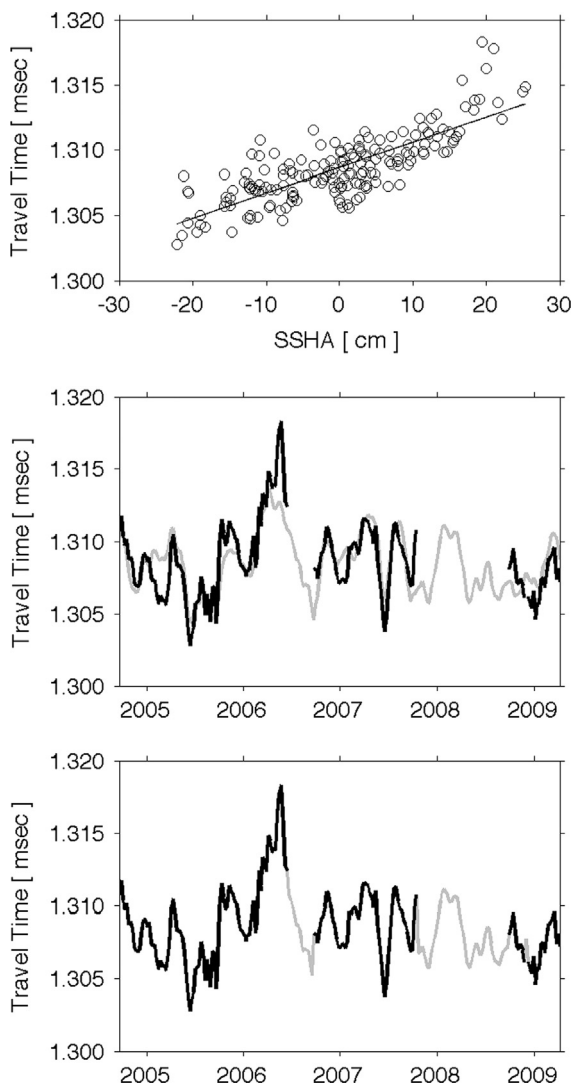


Fig. A1. Top: Illustration of the correlation ($r=0.8$) between the PIES-measured travel time at Site E and the sea surface height anomaly (SSHA) derived from the nearest grid-location in the gridded AVISO altimetry product. Middle: The time series of PIES-measured travel time (black line) and the regression-fit time series derived from the SSHA (gray line). Bottom: The final filled time series record where the largest gaps have been filled.

References

- Bower, A.S., Lozier, M.S., Gary, S.F., Boning, C.W., 2009. Interior pathways of the North Atlantic Meridional Overturning Circulation. *Nature* 459, 243–248, <http://dx.doi.org/10.1038/nature07979>.
- Bower, A., Lozier, S., Gary, S., 2011. Export of Labrador Sea water from the subpolar North Atlantic: a Lagrangian perspective. *Deep Sea Res. II* 58, 1798–1818.
- Chave, A.D., Luther, D.S., Filloux, J.H., 1997. Observations of the boundary current system at 26.5°N in the Subtropical North Atlantic Ocean. *J. Phys. Oceanogr.* 27 (9), 1827–1848.
- Chelton, D.B., Schlax, M.G., 1996. Global observations of oceanic Rossby Waves. *Science* 271, 234–238.
- Cunningham, S.A., T. Kanzow, D. Rayner, M.O. Baringer, W.E. Johns, J. Marotzke, H.R. Longworth, E.M. Grant, J.J.-M. Hirschi, L.M. Beal, C.S. Meinen, and H.L. Bryden, Temporal variability of the Atlantic Meridional Overturning Circulation at 26.5°N, *Science*, 317, 935, <http://dx.doi.org/10.1126/science.1141304>, 2007.
- Dengler, M., Schott, F.A., Eden, C., Brandt, P., Fischer, J., Zantopp, R., 2004. Break-up of the Atlantic Deep Western Boundary Current into eddies at 8°S. *Nature* 432, 1018–1020.
- Donohue, K.D., Watts, D.R., Tracey, K.L., Greene, A.D., Kennelly, M., Mapping circulation in the Kuroshio Extension with an array of current and pressure recording inverted echo sounders, *J. Atmos. Ocean. Technol.*, 27, 507–527, <http://dx.doi.org/10.1175/2009JTECHO686.1>, 2010.
- Emery, W.J., Thomson, R.E., 1997. *Data Analysis Methods in Physical Oceanography*. Pergamon Press, Oxford.
- Garzoli, S.L., 1984. Modes of variability of the 1983 thermocline signal. *Geophys. Res. Lett.* 11 (8), 741–744, <http://dx.doi.org/10.1029/GL011i008p00741>.
- Garzoli, S.L., Gordon, A.L., 1996. Origins and variability of the Benguela Current. *J. Geophys. Res.* 101 (C1), 897–906.
- Hendry, R.M., Watts, D.R., Meinen, C.S., 2002. Newfoundland Basin sea level variability from TOPEX/POSEIDON altimetry and inverted echo sounder/bottom pressure measurements. *Can. J. Remote Sens.* 28 (4), 544–555.
- Johns, W.E., Beal, L.M., Baringer, M.O., Molina, J.R., Cunningham, S.A., Kanzow, T., Rayner, D., 2008. Variability of shallow and Deep Western Boundary Currents off the Bahamas during 2004–05: results from the 26°N RAPID–MOC array. *J. Phys. Oceanogr.* 38, 605–623, <http://dx.doi.org/10.1175/2007JP03791.1>.
- Johns, W.E., Baringer, M.O., Beal, L.M., Cunningham, S.A., Kanzow, T., Bryden, H.L., Hirschi, J.J.-M., Marotzke, J., Meinen, C.S., Shaw, B., Curry, R., 2011. Continuous array-based estimates of Atlantic Ocean heat transport at 26.5°N. *J. Clim.* 24, 2429–2449, <http://dx.doi.org/10.1175/2010JCLI3997.1>.
- Kanzow, T., Cunningham, S.A., Rayner, D., Hirschi, J.J.-M., Johns, W.E., Baringer, M.O., Bryden, H.L., Beal, L.M., Meinen, C.S., Marotzke, J., 2007. Observed flow compensation associated with the meridional overturning at 26.5°N in the Atlantic. *Science* 317, 938, <http://dx.doi.org/10.1126/science.1141293>.

- Kanzow, T., Cunningham, S.A., Johns, W.E., Hirschi, J.J.-M., Marotzke, J., Baringer, M.O., Meinen, C.S., Chidichimo, M.P., Atkinson, C., Beal, L.M., Bryden, H.L., Collins, J., 2010. Seasonal variability of the Atlantic Meridional Overturning Circulation at 26.5°N. *J. Clim.* 23, 5678–5698, <http://dx.doi.org/10.1175/2010JCLI3389.1>.
- Lee, T.N., Johns, W., Schott, F., Zantopp, R., 1990. Western boundary current structure and variability East of Abaco, Bahamas at 26.5°N. *J. Phys. Oceanogr.* 20 (3), 446–466.
- Lee, T.N., Johns, W.E., Zantopp, R.J., Fillenbaum, E.R., 1996. Moored observations of western boundary current variability and thermohaline circulation at 26.5°N in the subtropical North Atlantic. *J. Phys. Oceanogr.* 26 (6), 962–983.
- Masumoto, Y., Sasaki, H., Kagimoto, T., Komori, N., Ishida, A., Sasai, Y., Miyama, T., Motoi, T., Mitsudera, H., Takahashi, K., Sakuma, H., Yamagata, T., 2004. A fifty-year eddy resolving simulation of the world Ocean – preliminary outcomes of OFES (OGCM for the Earth Simulator). *J. Earth Simulator* 1, 3556.
- McCarthy, G.D., Frajka-Williams, E., Johns, W., Baringer, M., Meinen, C., Bryden, H., Rayner, D., Duchez, A., Roberts, C., Cunningham, S., 2012. Observed interannual variability of the Atlantic Meridional Overturning Circulation at 26.5°N. *Geophys. Res. Lett.* 39, L19609, <http://dx.doi.org/10.1029/2012GL052933>.
- Meinen, C.S., Watts, D.R., 2000. Vertical structure and transport on a transect across the North Atlantic Current near 42°N: time series and mean. *J. Geophys. Res.* 105 (C9), 21869–21892.
- Meinen, C.S., Garzoli, S.L., Johns, W.E., Baringer, M.O., 2004. Transport variability of the Deep Western Boundary Current and the Antilles Current off Abaco Island, Bahamas. *Deep Sea Res.* 51, 1397–1415.
- Meinen, C.S., Baringer, M.O., Garzoli, S.L., 2006. Variability in Deep Western Boundary Current transports: preliminary results from 26.5°N in the Atlantic. *Geophys. Res. Lett.* 33, L17610, <http://dx.doi.org/10.1029/2006GL026965>.
- Meinen, C.S., Baringer, M.O., Garcia, R.F., 2010. Florida current transport variability: an analysis of annual and longer-period signals. *Deep Sea Res.* 57, 835–846.
- Meinen, C.S., Johns, W.E., Garzoli, S.L., van Sebille, E., Rayner, D., Kanzow, T., Baringer, M.O., 2013. Variability of the Deep Western Boundary Current at 26.5°N during 2004–2009. *Deep Sea Res.* 85, 154–168, <http://dx.doi.org/10.1016/j.dsr2.2012.07.036>.
- Molinari, R.L., Fine, R.A., Wilson, W.D., Curry, R.G., Abell, J., McCartney, M.S., 1998. The arrival of recently formed Labrador Sea water in the Deep Western Boundary Current at 26.5°N. *Geophys. Res. Lett.* 25 (13), 2249–2252.
- North, G.R., Bell, T.L., Cahalan, R.F., Moeng, F.J., 1982. Sampling errors in the estimation of empirical orthogonal functions. *Mon. Weather Rev.* 110, 699–706.
- Osychny, V., Cornillon, P., 2004. Properties of Rossby Waves in the North Atlantic estimated from satellite data. *J. Phys. Oceanogr.* 34 (1), 61–76.
- Rayner, D., Hirschi, J.J.-M., Kanzow, T., Johns, W.E., Wright, P.G., Frajka-Williams, E., Bryden, H.L., Meinen, C.S., Baringer, M.O., Marotzke, J., Beal, L.M., Cunningham, S.A., 2011. Monitoring the Atlantic Meridional Overturning Circulation. *Deep Sea Res.* 58, 1744–1753, <http://dx.doi.org/10.1016/j.dsr2.2010.10.056>.
- Riser, S.C., Freeland, H., Rossby, H.T., 1978. Mesoscale motions near the deep western boundary of the North Atlantic. *Deep Sea Res.* 25, 1179–1191.
- Rossby, T., 1969. On monitoring depth variations of the main thermocline acoustically. *J. Geophys. Res.* 74 (23), 5542–5546.
- Sasaki, H., Nonaka, M., Sasai, Y., Uehara, H., Sakuma, H., 2008. An eddy-resolving hindcast simulation of the Quasiglobal Ocean from 1950 to 2003 on the Earth Simulator. In: Hamilton, K., Ohfuchi, W. (Eds.), *High Resolution Numerical Modelling of the Atmosphere and Ocean*, Eds. Springer, New York, pp. 157–185.
- Schott, F.A., Dengler, M., Zantopp, R., Stramma, L., Fischer, J., Brandt, P., 2005. The shallow and deep western boundary circulation of the South Atlantic at 5–11°. *J. Phys. Oceanogr.* 35, 2031–2053.
- van Sebille, E., Baringer, M.O., Johns, W.E., Meinen, C.S., Beal, L.M., de Jong, M.F., van Aken, H.M., 2011. Propagation pathways of Classical Labrador Sea Water from its source region to 26°N. *J. Geophys. Res.* 116, C12027, <http://dx.doi.org/10.1029/2011JC007171>.
- Smith, W.H.F., Sandwell, D.T., 1997. Global sea floor topography from satellite altimetry and ship depth soundings. *Science* 277 (5334), 1956–1962.
- Stommel, H., 1957. A survey of Ocean current theory. *Deep Sea Res.* 4, 149–184.
- Stommel, H., Arons, A.B., 1960. On the abyssal circulation of the world Ocean – II. An idealized model of the circulation pattern and amplitude in oceanic basins. *Deep Sea Res.* 6, 217–233.
- Stouffer, R.J., Yin, J., Gregory, J.M., 2006. Investigating the causes of the response of the thermohaline circulation to past and future climate changes. *J. Clim.* 19 (8), 1365–1387.
- Swallow, J.C., Worthington, L.V., 1961. An observation of a deep countercurrent in the western North Atlantic. *Deep Sea Res.* 8, 1–19.
- Toole, J.M., Curry, R.G., Joyce, T.M., McCartney, M., Peña-Molino, B., 2011. Transport of the North Atlantic Deep Western Boundary Current about 39°N, 70°W: 2004–2008. *Deep Sea Res.* 58, 1768–1780.
- Vellinga, M., Wood, R.A., 2002. Global climatic impacts of a collapse of the Atlantic thermohaline circulation. *Clim. Change* 54 (3), 251–267.
- Wallace, J.M., Dickinson, R.E., 1972. Empirical orthogonal representation of time series in the frequency domain. Part I: theoretical considerations. *J. Appl. Meteorol.* 11, 887–892.
- Watts, D.R., Rossby, H.T., 1977. Measuring dynamic heights with inverted echo sounders: results from MODE. *J. Phys. Oceanogr.* 7, 345–358.
- Watts, D.R., Kontoyiannis, H., 1990. Deep-Ocean bottom pressure measurement: drift removal and performance. *J. Atmos. Ocean. Technol.* 7 (2), 296–306.
- Watts, D.R., Sun, C., Rintoul, S., 2001. A two-dimensional gravest empirical mode determined from hydrographic observations in the Subantarctic Front. *J. Phys. Oceanogr.* 31 (8), 2186–2209.